

JGR Atmospheres

RESEARCH ARTICLE

10.1029/2022JD038039

Key Points:

- Absorption of solar radiation helps to raise the altitude of black carbon aerosol by increasing buoyancy and vertical ascent
- This self-lofting mechanism has been captured in a climate model where radiative heating affects the large-scale ascent and circulation
- Self-lofting increased the altitude and long-range transport of black carbon to remote regions and the upper troposphere

Supporting Information:

Supporting Information may be found in the online version of this article.

Correspondence to:

B. T. Johnson,
ben.johnson@metoffice.gov.uk

Citation:

Johnson, B. T., & Haywood, J. M. (2023). Assessing the impact of self-lofting on increasing the altitude of black carbon in a global climate model. *Journal of Geophysical Research: Atmospheres*, 128, e2022JD038039. <https://doi.org/10.1029/2022JD038039>

Received 18 OCT 2022

Accepted 8 APR 2023

Author Contributions:

Conceptualization: B. T. Johnson, J. M. Haywood

Data curation: B. T. Johnson

Investigation: B. T. Johnson

Methodology: B. T. Johnson

Supervision: J. M. Haywood



Writing – original draft: B. T. Johnson

Writing – review & editing: J. M. Haywood

Haywood

© 2023 Crown copyright. © 2023 American Geophysical Union. All Rights Reserved. This article is published with the permission of the Controller of HMSO and the King's Printer for Scotland.

Assessing the Impact of Self-Lofting on Increasing the Altitude of Black Carbon in a Global Climate Model

B. T. Johnson¹  and J. M. Haywood^{1,2} 

¹Met Office Hadley Centre, Exeter, UK, ²College of Engineering, Mathematics, and Physical Sciences, University of Exeter, Exeter, UK

Abstract Black carbon (BC) absorbs solar radiation, increasing the buoyancy and vertical ascent of absorbing aerosol in the atmosphere. This self-lofting process has been observed for individual plumes in the troposphere and lower stratosphere but here we show it occurring at broader scales through enhanced large-scale ascent over BC-rich regions. This is demonstrated in a pair of simulation using the UKESM1 Earth-System model where BC aerosols were modeled either with or without the ability to absorb radiation. With absorption included the annual global mean concentration of BC in the upper troposphere and lower stratosphere (8–22 km) rose by up to 50% and the column loading over some remote oceanic regions more than doubled. The increase in aerosol height was particularly notable over the southeast Atlantic where biomass burning aerosol from Africa was elevated up to 1 km higher when their absorption was included. Similar effects were seen over the Arctic where the absorbing haze was transported in at higher levels and surface concentrations were halved. The absorption by BC also increased ascent over southern Asia, which tended to thicken the Asian brown cloud during the dry season but in the wet season enhancing ascent promoted deep convection and had the tendency to deplete the aerosol through wash-out. We conclude that representing aerosol absorption accurately is important in simulating the vertical distribution, transport and abundance of aerosol in the Earth-system that will affect their interactions with climate.

Plain Language Summary Black carbon is an important component of atmospheric aerosols as it absorbs solar radiation thereby heating the atmosphere and potentially warming climate. The localized heating can also affect clouds and atmospheric motions making the regional and climate effects more complex and uncertain. The vertical distribution and geographic spread of the aerosol is also key to how it interacts with the climate system. In this paper we highlight the fact that the absorption taking place in BC aerosols can affect its vertical ascent in the atmosphere and therefore how it becomes distributed across the globe. This self-lofting process was demonstrated in a climate model and was particularly important in aiding the elevation and downwind transport of absorbing smoke layers from regions such as central Africa, as well as increasing the amount of BC reaching the upper troposphere and lower stratosphere.

1. Introduction

Black carbon (BC) is a unique component of atmospheric aerosol that strongly absorbs solar radiation and thereby exerts a positive radiative forcing on the climate system with the potential to increase global temperatures (Bond et al., 2013; Myhre et al., 2013; Ramanathan & Carmichael, 2008; Stjern et al., 2017; Zhang & Wang, 2011). By locally heating the air BC can also affect the distribution of clouds, convection and precipitation by altering atmospheric temperatures and dynamical processes, ranging from boundary layer mixing to shifts in global and regional circulation patterns (Ackerman et al., 2000; Allen et al., 2012; Koch & Del Genio, 2010; Kovilakam & Mahajan, 2015; Myhre et al., 2018; Wang, 2013). Such impacts have been difficult to constrain owing to the complexity of the radiative and dynamical feedbacks involved (e.g., Johnson et al., 2019; Ming et al., 2010; Smith et al., 2018), many of which are dependent on the vertical distribution of the BC in the atmosphere (Johnson et al., 2004; Samset & Myhre, 2015; Zarzycki & Bond, 2010). Accurately simulating the vertical extent of BC is therefore key to modeling its interactions and impacts on the climate system. The vertical extent of aerosols depends on a range of factors, mainly the injection height, convective mixing and large-scale circulation but the radiative heating associated with absorbing components can also influence the ascent rate by increasing the buoyancy of aerosol-laden air. This so-called “self-lofting” mechanism (sometimes also referred to as “self-lifting”) may elevate absorbing aerosols higher and further than they would otherwise be in the atmosphere.

Among other studies, self-lofting has been considered in the contexts of individual smoke plumes from large fires (e.g., Herring & Hobbs, 1994; Radke et al., 1990), distinct layers of absorbing haze in the free troposphere (e.g., Haywood et al., 2021), the impacts of absorbing aerosol in volcanic plumes (e.g., Muser et al., 2020), and as a consequence of nuclear conflict (Pausata et al., 2016). As outlined by Boers et al. (2010) and Ohneiser et al. (2023), the gain in elevation will depend on a range of factors, including the strength of aerosol absorption, the stability of the atmosphere and the length of time before the aerosol is dispersed or removed. In a relatively extreme example, Boers et al. (2010) showed self-lofting could raise an optically thick and highly absorbing aerosol layer to the tropopause in 3–4 days Moorthy et al. (2016) estimated slightly more modest ascent rates of 1 km per day for absorbing haze in the mid-troposphere above India. Most observational evidence for self-lofting has been associated with large wildfire events where thick smoke plumes have ascended to the upper troposphere or even into the stratosphere (Ansmann et al., 2021; Latt et al., 2012; Ohneiser et al., 2021) where they can persist for weeks or months (e.g., Damany-Pearce et al., 2022). Ohneiser et al. (2023) assessed self-lofting rates due to aerosol radiative heating by comparing satellite observations and detailed model calculations for major wildfire smoke event. In certain cases, pyrocumulus have been involved in lofting smoke to the tropopause and self-lofting has then aided the onward ascent of the aerosol into the stratosphere (Peterson et al., 2018; Torres et al., 2020; Yu et al., 2019, 2021). The Australian New Year fires event of December 2019–January 2020 was an extreme example of this, where a region of smoke ascended as high as 35 km within a self-induced vortex (Kablick et al., 2020; Khaykin et al., 2020).

The impact of self-lofting on broader or more dispersed aerosol layers is more difficult to infer observationally and so far, has not been well investigated but could have a significant role in the global distribution of absorbing aerosol. For instance, various studies have highlighted the impacts of BC absorption on atmospheric circulation (Bollasina et al., 2008; Johnson et al., 2019; Shen & Ming, 2018) and indicate enhances in vertical motion in polluted regions such as Southern Asia and Tropical Africa. The idealized simulations of Sand et al. (2015) also showed remarkable changes in the vertical extent and geographic spread of the BC after scaling up the emission of BC to induce very strong levels of absorption. This indicated that the absorption could affect the transport of the aerosol in a broad-scale climate model by preferentially enhancing large-scale vertical motion in regions with higher BC loadings.

Here we investigate to what extent self-lofting may affect BC transport in present-day climate simulations using the UKESM1 earth system model. Our model, like most other global models cannot resolve the dynamics associated with individual plumes but the radiative heating associated with the aerosol will have an impact on convective fluxes and mean ascent and therefore capture self-lofting at the gridbox scale. The experiment involves a pair of simulations representing present-day aerosol conditions where the absorption from BC has either been enabled or switched off in the radiation scheme. The model was run in coupled mode to enable feedback between aerosol absorption, atmospheric circulation and changes in sea surface temperature. Results focus initially on the global picture then investigate three regions of interest: southeast Atlantic, the Arctic and southern Asia.

2. Methods

2.1. Model Description

This study uses the first version of the UK Earth System Model (UKESM1.0) (Sellar et al., 2019) and most aspects of the implementation follow those used in the sixth Coupled Model Intercomparison Project (CMIP6) (Sellar et al., 2020). UKESM1 includes a fully coupled atmosphere, ocean, sea ice system based on the physical climate model HadGEM3-GC3.1 (Hadley Centre Global Environment Model version 3; Kuhlbrodt et al., 2018; Williams et al., 2018) with the addition of interactive land-vegetation, tropospheric and stratospheric chemistry and ocean biogeochemistry. Whilst much of the complexity in UKESM1 has no direct connection to aerosol-radiation processes and atmospheric circulation feedbacks, the choice of model ensures the results will be as relevant as possible to the kind of highly complex models that are typically used to assess aerosol-climate interactions.

UKESM1 includes the modal version of the Global Model of Aerosol Processes (GLOMAP-mode) (Mann et al., 2010). This represents the emission, transport and deposition of BC, organic matter, sulfate and sea salt across a range of soluble and insoluble size modes in which chemical components are internally mixed. Mineral dust is represented separately with a 6-bin scheme (Woodward et al., 2022). Whilst a detailed description and evaluation of the aerosol performance in UKESM1 is given in Mulcahy et al. (2020) and an assessment of the

aerosol processes and effective radiative forcings were presented in Mulcahy et al. (2018), some aspects of the aerosol simulation are also summarized below.

Emissions of BC and organic matter from the combustion of fossil fuels, biofuel and biomass burning are injected into an Aitken insoluble mode, and these subsequently age and mix with sulfate to join the soluble Aitken or accumulation modes. Biomass burning emissions from forested zones are injected aloft in a uniform layer between the surface and 3 km (approximately 700 hPa). This assumes a significant degree of plume rise from large fires. Other biomass burning and primary carbonaceous emissions are released at the lowest model level.

In relation to BC, UKESM1 includes an update to the refractive index, raising the value from 1.75–0.44i to 1.85–0.71i (Bond & Bergstrom, 2006). This increased absorption and when combined with CMIP6 emissions gives a relatively strong pre-industrial to present-day instantaneous radiative forcing of $+0.38 \text{ Wm}^{-2}$ (O'Connor et al., 2021). Effects of BC on snow albedo are not included in this model configuration. Absorption by organic matter is not included making BC the only aerosol component originating from anthropogenic and biomass-burning emissions that absorbs significantly in the solar spectrum. Evaluations of aerosol composition, optical depth and absorption properties were provided in Mulcahy et al. (2018) and Mulcahy et al. (2020). BC mass and Aerosol Absorption Optical Depth (AAOD) showed significant scatter between model and point observations but no substantial biases.

Aerosol radiative effects, including the heating from BC were calculated within the model's two-stream radiation scheme (Edwards & Slingo, 1996; Manners et al., 2022). This combines the scattering and absorption properties from aerosols, gases and clouds and resolves their impact on radiative fluxes and radiative heating rates in 6 solar and 9 terrestrial spectral bands at each model level within atmospheric columns. The radiative heating rates affect the dynamics of the atmosphere by altering the temperature (buoyancy) in grid cells at every 20-min time step. Self-lofting arises where BC radiative heating triggers increases in the vertical transport of aerosol by the resolved flow and/or by parameterized sub-grid scale turbulence and convection. This could include changes to the vertical mixing of aerosol in the boundary layer as radiative heating affects turbulence and boundary layer height.

Both GLOMAP-mode and the dust scheme include representations for dry deposition and scavenging by precipitation (rainout). For the soluble modes, GLOMAP-mode also includes nucleation scavenging from large-scale precipitating clouds (in-cloud scavenging) and moist convection (plume scavenging). In both schemes aerosol optical properties are calculated via Mie theory assuming homogeneous spheres. In GLOMAP-mode volume-weighted averaging is used to calculate the refractive index in each of the radiatively active modes. The dust aerosol and Aitken insoluble mode are assumed to be hydrophobic, whereas the particle properties in the soluble modes in GLOMAP-mode are used in the activation scheme (West et al., 2014), along with updraught velocities, to calculate cloud droplet number concentration at cloud base for the microphysics scheme. Impacts of these aerosol-microphysical processes on cloud brightness and cloud lifetime are thereby included in the model. Whilst BC may be present in the soluble modes only the sulfate, sea salt and organic matter attract water during wet growth and activation.

2.2. Experimental Design

The objective of this experiment was to assess how the absorption by BC affects the transport of aerosol through feedbacks between radiative heating and atmospheric circulation. In a previous set of idealized experiments Johnson et al. (2019) showed very substantial changes to the large-scale circulation when anthropogenic BC emissions were increased by a factor of 10 in an atmosphere-only version of UKESM1. However, in this study we wanted to assess the scale of the impact in typical present-day conditions and gauge this by contrasting two simulations where absorption has either been included at normal levels (“Abs”) or switched off (“Non-abs”). This was achieved by setting the imaginary part of refractive index for BC to zero in the Non-abs simulation. Absorption by organic carbon (i.e., brown carbon) is not included in UKESM1 so was zero in both simulations. Emissions of BC and primary organic carbon were set to present-day values (2014) based on CMIP6 (Hoesly et al., 2018; Sellar et al., 2020). This set up included emissions of biomass burning from the Global Fire Emissions database version 4 (GFED4), likewise from the year 2014 to represent typical present-day conditions. To enable a long integration with minimal drift in sea surface temperatures the model was initialized from fully spun-up pre-industrial control run and all other forcings, emissions and greenhouse gas concentrations were

maintained at 1850 levels. This experimental setup is similar to that used in the CMIP6 Aerosol-Chemistry Model Intercomparison Project (AerChemMIP) experiment designed to evaluate preindustrial to present day BC forcing (code named “piClim-BC”) (Collins et al., 2017; O’Connor et al., 2021), except that in our simulations ocean and land-surface vegetation feedbacks are included as well as the more rapid atmospheric adjustments to BC heating (or lack thereof). The simulations were run for 125 years each (much longer than in O’Connor et al., 2021) and impacts were assessed by comparing averages from the final 50 years. The statistical significance of results was tested using a one-sample student’s *t*-test based on the variance of annual means. The simulation data and the python programs used to analyze and visualize it are accessible via Johnson (2022).

2.3. Calculation of Aerosol Layer Height

In parts of the analysis, we assess the mass-weighted mean altitude of BC aerosol, which indicates a representative height (Z_{aer}) for the aerosol layer. This was calculated from the following equation, where z is altitude above sea level, m_{aer} is the mass concentration of aerosol (kg/m^3), and z_t was set to 25 km, above which aerosol concentrations were negligible.

$$Z_{\text{aer}} = \frac{\int_0^{z_t} m_{\text{aer}} * z \, dz}{\int_0^{z_t} m_{\text{aer}} \, dz} \quad (1)$$

In some instances, we assess Z_{aer} for the BC aerosol (where m_{aer} is the BC mass concentration) and in other instances we assess Z_{aer} for the carbonaceous aerosol (where m_{aer} is the sum of BC and organic matter) to assess the impact of the lofting on the carbonaceous aerosol as a whole.

3. Analysis of Global Impacts

3.1. Global Distribution of Absorbing Aerosol and Its Radiative Effects

Figure 1a shows the global distribution of annual mean AAOD of BC from the control simulation, giving a column-integrated metric of the BC absorption. The regions most affected are central Africa and southern and eastern Asia where there are strong BC emissions from biomass burning (Africa), biofuel (southern Asia) and fossil-fuel combustion (east Asia). Smaller hot spots of BC AAOD are found in other biomass burning regions such as in Amazonia, northern Canada and Siberia. As there is strong seasonality in emissions, particularly from biomass burning, the AAODs may be considerably higher in peak months compared to the annual mean shown in the figure. Since we only perturb the BC absorption in the experiment the plotted field only shows the BC contribution to AAOD, as an indication of where changes in aerosol lofting rates might be expected. Mineral dust absorption was included in both simulations equally and accounted for about 10% of the global annual mean AAOD but that contribution was excluded in the plot.

The radiative impacts of including BC absorption were evaluated from the final 50 years of the simulations to place these results of this paper in context, in terms of the magnitude of the radiative perturbation between the Abs and Non-abs simulations (see Table 1). The inclusion of BC absorption in the Abs experiment led to a 2.44 Wm^{-2} increase in absorption within the atmosphere relative to the Non-abs simulation (Figure 1b). This is based on the direct (instantaneous) radiative effect of the aerosol calculated using radiation calls with and without aerosol-radiation interactions (as in Ghan et al., 2012 and Johnson et al., 2019). The spatial distribution of BC absorption (Figure 1b) largely corresponds to the distribution of BC AAOD (Figure 1a) and emphasizes that the strongest potential for increasing the buoyancy and vertical motion (i.e., lofting) are in Tropical Africa and Southern–Eastern Asia. The radiative absorption by BC aerosol-radiation interactions also leads to a $+0.96 \text{ Wm}^{-2}$ change in net radiation at the top of the atmosphere (TOA) and a -1.48 Wm^{-2} change in radiation absorbed at the surface (the TOA effect is the increase in atmospheric absorption plus the change in surface absorption). Note that the instantaneous radiative effect at the TOA of $+0.96 \text{ Wm}^{-2}$ that is found here is stronger than the instantaneous radiative forcing of $+0.38 \text{ Wm}^{-2}$ (O’Connor et al., 2021) because the latter is diagnosed as the change in the TOA radiation budget between present day and 1850, rather than the change between present day and no BC absorption at all. The changes in net radiation due to BC aerosol-radiation interactions were strongly dominated by the shortwave component. However, over time fast and slow feedbacks in the climate system led to radiative adjustments in both the shortwave and longwave budget (e.g., Samset et al., 2016). These

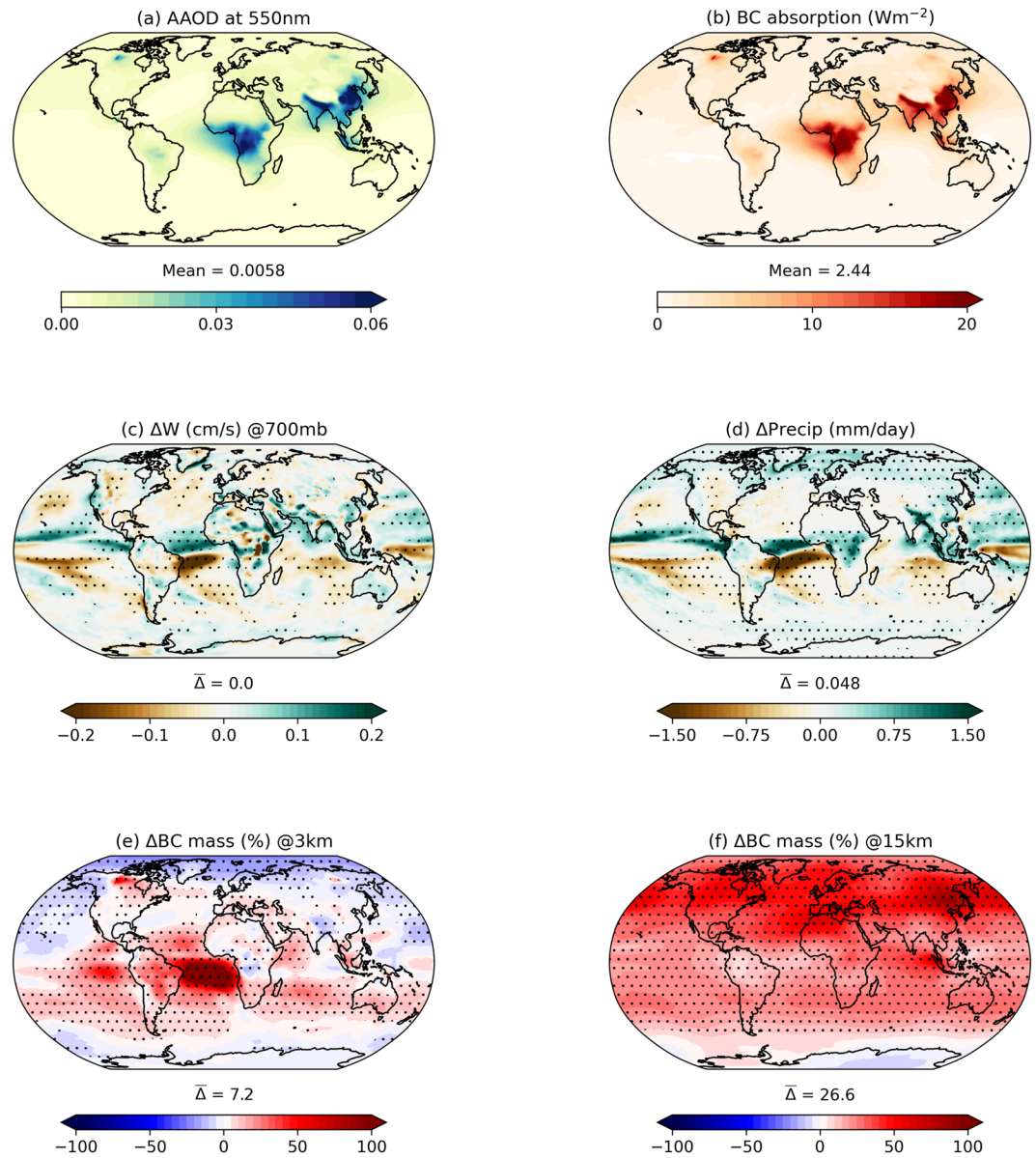


Figure 1. Impacts of including black carbon (BC) absorption, based on the annual mean differences between the Abs and Non-abs simulations. Plots include the changes in (a) absorption aerosol optical depth at 550 nm, (b) net radiative absorption throughout the atmospheric column from aerosol-radiation interactions, (c) vertical velocity at 700 mb (~ 3 km) (cm s^{-1}), (d) precipitation (mm/day), and relative changes in BC mass concentration at (e) 3 km and (f) 15 km. Global means are indicated under the map with $\bar{\Delta}$ indicating the global mean change due to self-lofting. Stipples indicate where the changes are statistically significant at the 95% confidence level.

Table 1
Changes in Net Radiation Due To Including BC Absorption (Abs–Non-abs)

Instantaneous radiative effect of BC absorption			Change in net radiation after fast and slow adjustments
TOA	SFC	ATM	TOA
0.96	–1.48	2.44	0.33

Note. Values given in Wm^{-2} , evaluated at the top of atmosphere (TOA), across the atmosphere (ATM), and at the surface (SFC) and were averaged over the final 50 years of the simulations.

adjustments stem from changes to clouds, atmospheric temperature, water vapor and surface albedo and altogether reduce the difference in net TOA radiation between the Abs and Non-abs simulations to 0.33 Wm^{-2} by the final 50 years of the experiment.

3.2. Lofting at the Global Scale

The absorption associated with BC does lead to statistically significant in changes in vertical motion, as indicated by the difference in annual mean vertical velocity at 700 mb, shown in Figure 1c. Statistically significant

changes (stippled in the figure) occur quite widely across the globe, with strong increases of $0.1\text{--}0.3\text{ cm s}^{-1}$ associated with the absorbing aerosol plumes over Africa, the tropical Atlantic and over southern and eastern Asia. These rates of ascent would correspond to an elevation of $86\text{--}260\text{ m day}^{-1}$ or approximately $0.5\text{--}1.5\text{ km}$ over 5 days, which is the average lifetime of BC aerosol in the model. They are therefore strong enough to make a significant impact on the vertical transport of aerosol. Compensating descent occurs in other regions, particularly the tropical and sub-tropical oceans in the southern hemisphere, which induces a reduction in precipitation. The pattern of increased ascent in the northern tropics and descent south of the equator is indicative of a northward shift in the ITCZ toward the hemisphere with greater BC heating. This shifting of the ITCZ toward the warmer hemisphere has been documented in earlier versions of the model (e.g., Haywood et al., 2013, 2016; Hawcroft et al., 2017) and has been extensively studied in idealized aquaplanet (e.g., Voigt et al., 2013, 2014) and other fully coupled climate models (e.g., Frierson et al., 2013) and is caused by an enhanced cross-equatorial energy transport from the warmer to the colder hemisphere in the upper branches of the Hadley cell. This transport of energy enhances near-surface moisture transport in the lower branches of the Hadley cell from the colder to the warmer hemisphere enhancing moisture supply to the monsoon circulation, leading to a shift in the ITCZ (e.g., Hwang & Frierson, 2013). The associated changes in vertical velocity in our Abs simulation are also accompanied by marked shifts in annual mean precipitation (Figure 1d) with decreases in the southern tropics and increases in the northern tropics and regions such as Central Africa and Southern Asia where the BC absorption was particularly strong. The moderate increases in the high latitudes were a result of a general warming of the atmosphere-ocean system and associated slow feedbacks on the climate, rather than lofting induced by the BC absorption.

As expected, the increases in vertical velocity at 700 mb ($\sim 3\text{ km}$) are accompanied by increases in BC mass concentration (Figure 1e) as aerosol is lofted out of the boundary layer and into the lower free troposphere. The BC concentration at this altitude has increased by around 8% in the global annual mean, but bigger increases of 50%–100% are seen downwind of biomass burning aerosol sources, most notably over the tropical and southeastern regions of the Atlantic, but also in northern Canada, Siberia, and southeast Asia. There are also moderate increases (10%–20%) over most tropical and sub-tropical ocean regions but slight decreases ($\sim 10\%$) over the north Pacific and the polar regions. A few regions over land (central Africa and the Middle East) show slight decreases in BC concentration at 700 mb and there are some decreases over the North Pacific and at higher latitudes. The changes in BC mass are statistically significant at the 95% confidence level in most areas, as indicated by the stippling on the map indicating that self-lofting has had a clear influence on the global distribution of BC. There are also increases in BC mass higher up in the upper troposphere and lower stratosphere, as indicated in Figure 1f, showing the relative change at 15 km. The relative increases at that altitude are stronger (27% globally) but the spatial pattern of change is more ubiquitous rather than showing a connection to regions with high AAOD (Figure 1a) or enhanced low-level ascent (Figure 1c).

3.3. Changes in the Vertical Distribution of BC Mass

Figure 2 examines the changes in BC vertical distribution further by showing the global mean profiles and zonal-mean cross-sections of BC in the simulations and the impact of including absorption. Self-lofting has increased the global mean BC mass concentrations between 2 and 5 km by around 5%, but larger relative increases of up to 50% occur in the upper troposphere and lower stratosphere (8–22 km) (Figures 2a and 2b) where there appears to be an upward shift in the height that BC attains, before the concentrations tail off more rapidly in the stratosphere. This was consistent with increases in the height of the tropopause in the Abs simulation (here diagnosed from the thermal gradient, according to WMO, 1992). The annual global mean height of the tropopause increases by 190 m in Abs, relative to Non-abs and there were zonal mean increases of around 300 m in the northern hemisphere mid-high latitudes ($30\text{--}90^\circ\text{N}$) (Figure S1a) where there were higher concentrations of BC in the upper troposphere (Figure 2c). Even greater increases of up to 500 m were seen at 40°N during JJA (Figure S1b). Since the absolute BC mass concentration is declining rapidly with height the increases at higher altitudes become smaller in absolute terms and the main mass transfer has been a redistribution of BC between the BL and the lower troposphere (2–5 km) (Figure 2b). In the zonal mean difference plot (Figure 2d) it is clear there has been some depletion of BC from the boundary layer ($<2\text{ km}$) in the tropics and 20%–50% increases above it. Increases in BC loadings at upper levels are also seen over the mid and high latitudes with the maximum relative increases just above the tropopause. The changes shown here indicate that radiative absorption enables BC-rich layers to somewhat overcome or penetrate the stratification barrier at the tropopause, as well as the

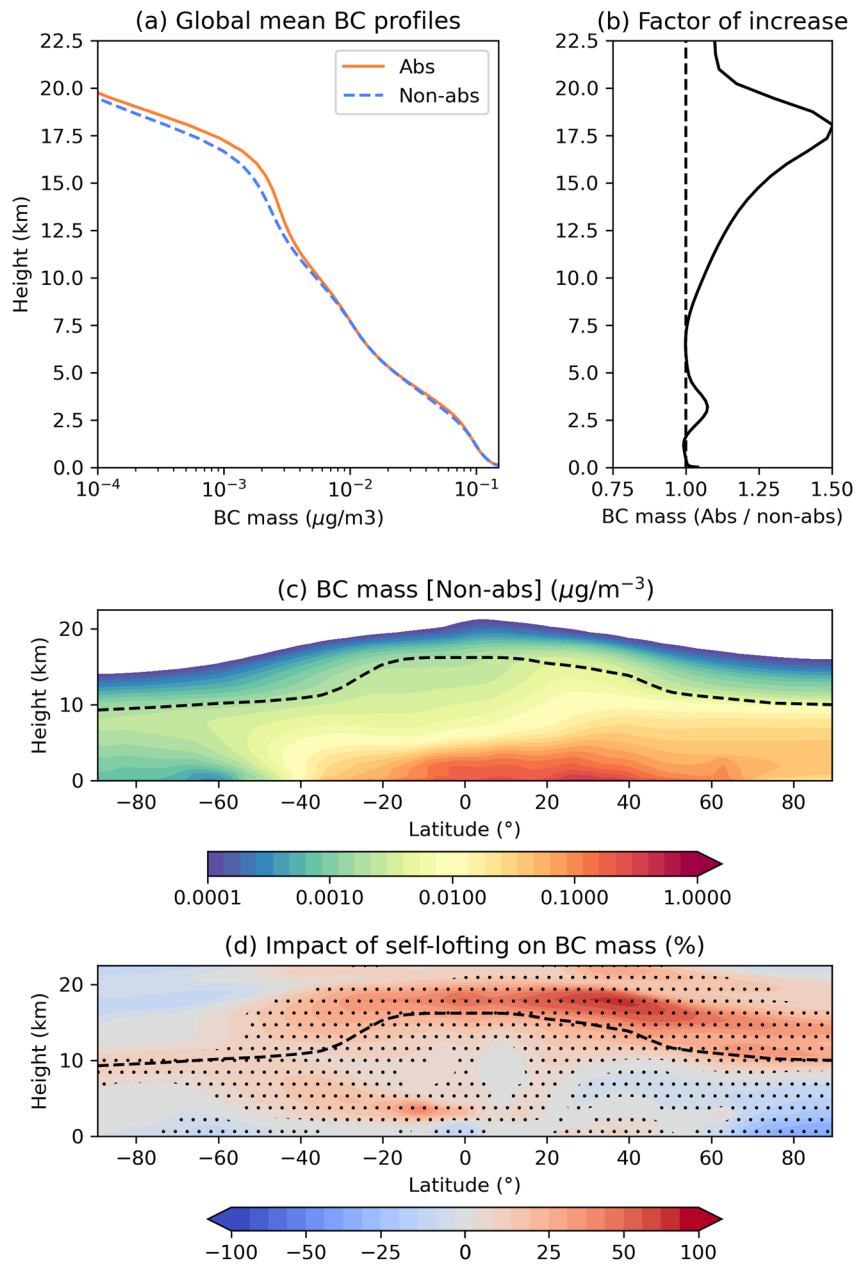


Figure 2. Impact of self-lofting on the vertical distribution of black carbon (BC) at the global scale. Plots include (a) global annual mean profile of BC mass as a function of altitude from the Abs and Non-abs simulations, (b) the ratio between the two profiles (Abs/Non-abs), (c) annual zonal mean BC mass concentration (g/m^3) from the Non-abs simulation, and (d) the change in BC mass due to self-lofting given as the relative difference (%) between the Abs and non-abs simulations. Stipples indicate where the changes are statistically significant at the 95% confidence level.

capping inversion typically found at the top of the boundary layer. Since the BC concentration drops strongly in absolute terms with height the lofting rate is likely slower in the higher layers and some of the changes in vertical transport may be due to large-scale adjustments in the circulation rather than localized heating. The additional aerosol concentrations in the stratosphere will also increase heterogeneous ozone depletion and solar absorption will increase the temperature at the tropopause, reducing the efficiency of the water vapor cold-trap leading to increased water vapor in the stratosphere which will increase ozone destruction (via catalytic HOx reactions), which will influence stratospheric temperatures and dynamics. Examining such complex couplings are beyond the scope of the paper and are dealt with more comprehensively by Haywood et al. (2022). Whatever the precise balance of mechanisms, increasing the amount of aerosol that reaches the free troposphere and lower stratosphere

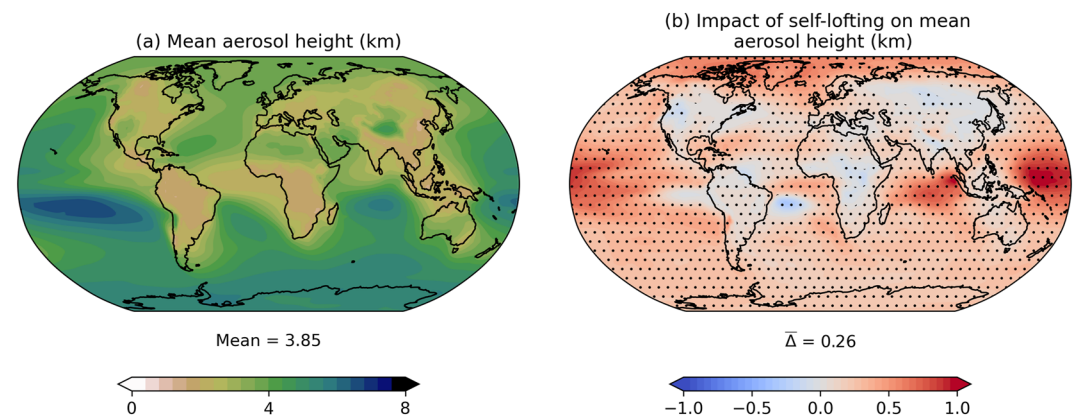


Figure 3. Annual mean aerosol layer height (km) for carbonaceous aerosol (BC + OC), calculated as the mass-weighted mean altitude of the aerosol. Results are for (a) the Non-abs simulation, (b) the change due to self-lofting (Abs–Non-Abs). Global means are indicated under the map with $\bar{\Delta}$ indicating the global mean change due to self-lofting. Stipples indicate where the changes are statistically significant at the 95% confidence level.

could lead to a range of impacts on cloud microphysical processes, aerosol-radiation interactions and atmospheric chemistry. Overall, the global mass loading of BC increased by 3.4% due to the self-lofting and the atmospheric lifetime of BC would also have implicitly increased by that percentage.

3.4. Changes in Aerosol Layer Height

Figure 3 provides a further view on how self-lofting affected the vertical extent of absorbing aerosol across the globe. These plots show the mass-weighted mean altitude of carbonaceous aerosol (BC + OC), as defined in Section 2.3. This provides a representative height for the aerosol layer as a whole and emphasizes that other co-emitted species (namely the organics) are lofted along with the BC. In the control simulation the aerosol height tends to be around 2–3 km over source regions and rises to 4–7 km over more remote oceanic regions. On including BC absorption the aerosol height rises by an average of 260 m, but there are increases of up to 1 km in the most affected regions. On the whole the changes are small or neutral over continents but positive over oceans with the biggest increases over remote oceanic regions such as Indian Ocean, tropical west Pacific where carbonaceous aerosol mainly arrives in elevated layers. During long-range transport self-lofting may have more time to take effect leading to the biggest altitude gains.

4. Analysis of Regional Changes

4.1. Impacts Over the Southeast Atlantic During Biomass Burning Season

The largest region of absorbing aerosol in the simulations is by far the biomass burning aerosol plume over the tropical and southeastern regions of the Atlantic (Figure 1). This originates from fires over central and southern Africa that peak during August–October. The absorbing layers typically reside above brightly reflective decks of marine stratocumulus leading to an overall positive radiative forcing from aerosol-radiative interactions (de Graaf et al., 2020; Keil & Haywood, 2003). If the aerosol descends sufficiently through subsidence it can entrain into the marine boundary layer affecting cloud microphysical properties and induce a negative radiative effect from aerosol-cloud interactions (Redemann et al., 2021). On the other hand, radiative absorption above the cloud can act to reduce cloud top entrainment and thicken the cloud layer (Herbert et al., 2020; Johnson et al., 2004), which has a negative radiative effect. The balance between these competing aerosol effects is uncertain and depends on the level of absorption (Mallet et al., 2020) and the vertical placement of the aerosol layer relative to the cloud (Gupta et al., 2021). As such absorption-lofting could have a key influence on aerosol-cloud-radiation interactions in this region. Since the radiative effects and cloud interactions from this smoke aerosol also play a role in modulating precipitation over the wider region, including the West African Monsoon (Ajoku et al., 2019; Randles & Ramaswamy, 2010; Sakaeda et al., 2011; Solmon et al., 2021) any change in the transport and lifetime of such layers, due to lofting, could have broader impacts on regional climate.

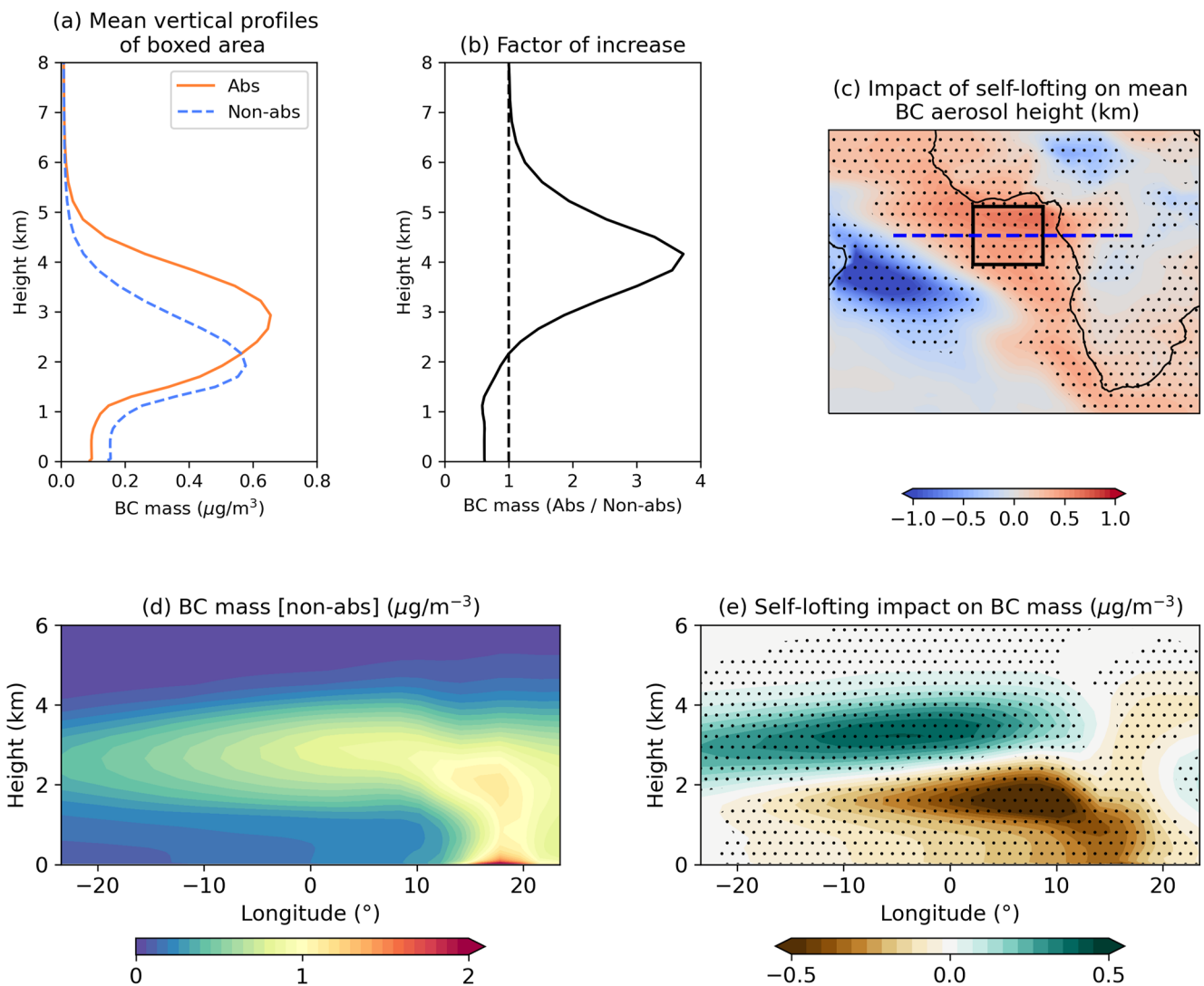


Figure 4. Impact of self-lofting on the distribution of black carbon (BC) mass over the southeast Atlantic during August–September. The profiles show (a) BC aerosol mass as a function of height from the Abs and non-abs simulations, based on data from the boxed region on the map (7.5°E–5°W, 7.5°S–2.5°N) and (b) the ratio of the two profiles (Abs/Non-abs). The map (c) shows the change in mass-weighted mean aerosol height (km) for carbonaceous aerosol (BC + OC). The cross-sections show (d) BC aerosol mass concentration ($\mu\text{g}/\text{m}^3$) from the Non-abs simulation and (e) the change due to self-lofting (Abs–Non-abs) along a line of 25°E–25°W and 2.5°S (dashed line in subplot c). Stipples indicate where the changes are statistically significant at the 95% confidence level.

The results shown in Figure 4 are evaluated for August–September rather than the annual mean, corresponding to the time that the southeast Atlantic haze layer typically peaks. The analysis shows that the biomass burning aerosol layer has lofted 0.5 km higher in the region off the coast of central and southern Africa (Figures 4a and 4c) after including BC absorption. The vertical profile (Figure 4a) shows a clear upward shift in the aerosol vertical distribution leading to a greater proportion of the BC mass residing above 2 km where it is likely to be above any marine stratocumulus. For instance, the BC mass at 3–4 km increased by a factor of 2–3.5 (Figure 4b). It is difficult to prove that this degree of self-lofting occurs in the real world, but the Abs model simulation does better than the Non-abs simulation in reproducing the profile of aerosol extinction observed by Haywood et al. (2021) during the Cloud-Aerosol-Radiation Interaction and Forcing (CLARIFY) campaign launched from Ascension Island in the Tropical Atlantic (see Figure S2).

These shifts in the BC profile are likely to be important in how biomass burning aerosol affects radiation and clouds over the southeast Atlantic. Absorbing aerosols above marine stratocumulus have the potential to exert a strong positive direct radiative effect via aerosol-radiation interactions, and to stabilize the cloud layer via the semi-direct effect. Furthermore, the concentration of BC in the boundary layer at 1 km decreased by about

40%, indicating that self-lofting could lead to less aerosol entraining into the marine boundary layer, weakening microphysical aerosol-cloud interactions. The cross-sections in Figures 4d and 4e indicate that the absorption raises the plume over the continent so that less mixes into the marine boundary layer near the coast and more of it is transported out at higher elevations. Further studies would be useful to evaluate how important the change in vertical elevation might be for these aerosol-radiation and aerosol-cloud interactions in the region. Another aspect might be to investigate how the lofting affects broader climate responses, such as changes to precipitation patterns in the region. In our simulations, BC absorption increases annual mean precipitation over the tropical zone of the African continent and leads to a northward shift of the ITCZ over the tropical Atlantic (Figure 1d and Figure S3a). The modeled precipitation increases over Africa were stronger during August–September when the biomass burning emissions from central and Southern Africa peaked (see Figure S3b). However, it is not clear from our experiments how sensitive these precipitation responses are to the altitude of the BC heating.

4.2. Impacts on Arctic Haze During Summertime

Absorbing aerosol haze layers are commonly found over the Arctic, especially during the summer months (e.g., Quinn et al., 2007; Shaw, 1995) and originate from a range of sources, including industrialized zones in the northern Hemisphere, biomass burning events in the Boreal forest (e.g., Xian et al., 2022) and to a lesser extent localized sources in and around the Arctic perimeter (Law & Stohl, 2007; Stohl et al., 2013; Zheng et al., 2021). The haze typically arrives in elevated layers but can mix down into the boundary layer and interact with mixed-phase clouds. During 2019, elevated aerosol layers were observed over the high Arctic at altitudes of 7–18 km and were attributed to self-lofted smoke originating from Siberian wildfires during 2019 (Ohneiser et al., 2021), although others have attributed the elevated aerosol to volcanic aerosol from the Raikoke eruption (Boone et al., 2022). Aerosol in the Arctic are important for climate forcing as it affects the radiation balance directly, and the microphysical properties of low-level mixed-phase clouds (Lohmann, 2017). BC also reduces the reflectance of the surface as it deposits on snow and ice (e.g., Kang et al., 2020), although this impact is not included in our simulations.

The analysis in Figure 5 focusses on the impacts of self-lofting in the high latitude zone of 60–90°N during the months of June–August when solar illumination is high (enabling strong absorption) and there is significant advection of BC into the Arctic. As shown in Figure 5a, the zonal mean BC concentration in the control simulation is highest ($\sim 0.2 \mu\text{g}/\text{m}^3$) south of 65°N and resides in a relatively well-mixed layer below 3 km. Further north, the BC concentration drops sharply at the lowest levels (0–1.5 km) but above this lies an elevated layer with more moderate concentrations ($0.05\text{--}0.1 \mu\text{g}/\text{m}^3$) extending across the pole. This pattern is consistent with the uplift of warmer and more polluted air from mid-latitudes followed by northward advection in large-scale eddies. In Figure 5b, we see that absorption has aided the uplift of the aerosol in the polluted zones to the south ($<70^\circ\text{N}$), reducing concentrations of BC in the lowest 1.5 km but increasing them from 1.5–3 km (Figure 5b). In the higher Arctic (70–90°N), the self-lofting has had the effect of raising the mean height of the BC aerosol (Figure 5c) but the total amount of BC in this layer below 6 km has slightly decreased. The decreases below 6 km are likely due to increases of precipitation and total column wet deposition (of around 10%) between 60–70°N (Figures S4 and S5), depleting the loading of aerosol in the tropospheric layer. Whilst the elevated aerosol layer still spreads out above the high Arctic the maximum concentration in the regional-mean profile (Figure 5c) is diminished from 0.090 to $0.067 \mu\text{g}/\text{m}^3$ and the altitude where the peak occurs has lifted by around 300 m. The concentration in the upper troposphere and lower stratosphere (6–12 km) increased (Figures 5b–5d), consistent with the broader pattern of an upward shift in the profile of BC concentration (Figure 2a) and an increase of approximately 400 m in the mean height of the tropopause across the Arctic during JJA (Figure S1b). This upward shift in the mean height of the aerosol occurs broadly across the whole region (Figure 5e). The surface mass concentration is reduced almost everywhere north of 60°N, and in the interior of the Arctic region there are reductions of around 50%–70% (Figure 5f), which tallies with the reduction shown in the mean profile (Figure 5d). The changes in column burden are a slightly different story (Figure 5g) with reductions of 20%–30% in the interior of the Arctic but increases around the perimeter. This reflects the competing effects from enhanced self-lofting and increased wet deposition resulting in less BC in the Arctic north of 70°N.

These changes could have complex effects on aerosol forcing in the region that could be explored in future work. In the high Arctic, the decline in BC column mass loading will likely reduce the magnitude of positive direct aerosol-radiation interactions occurring where absorbing haze lies above ice, snow, or brightly reflective clouds.

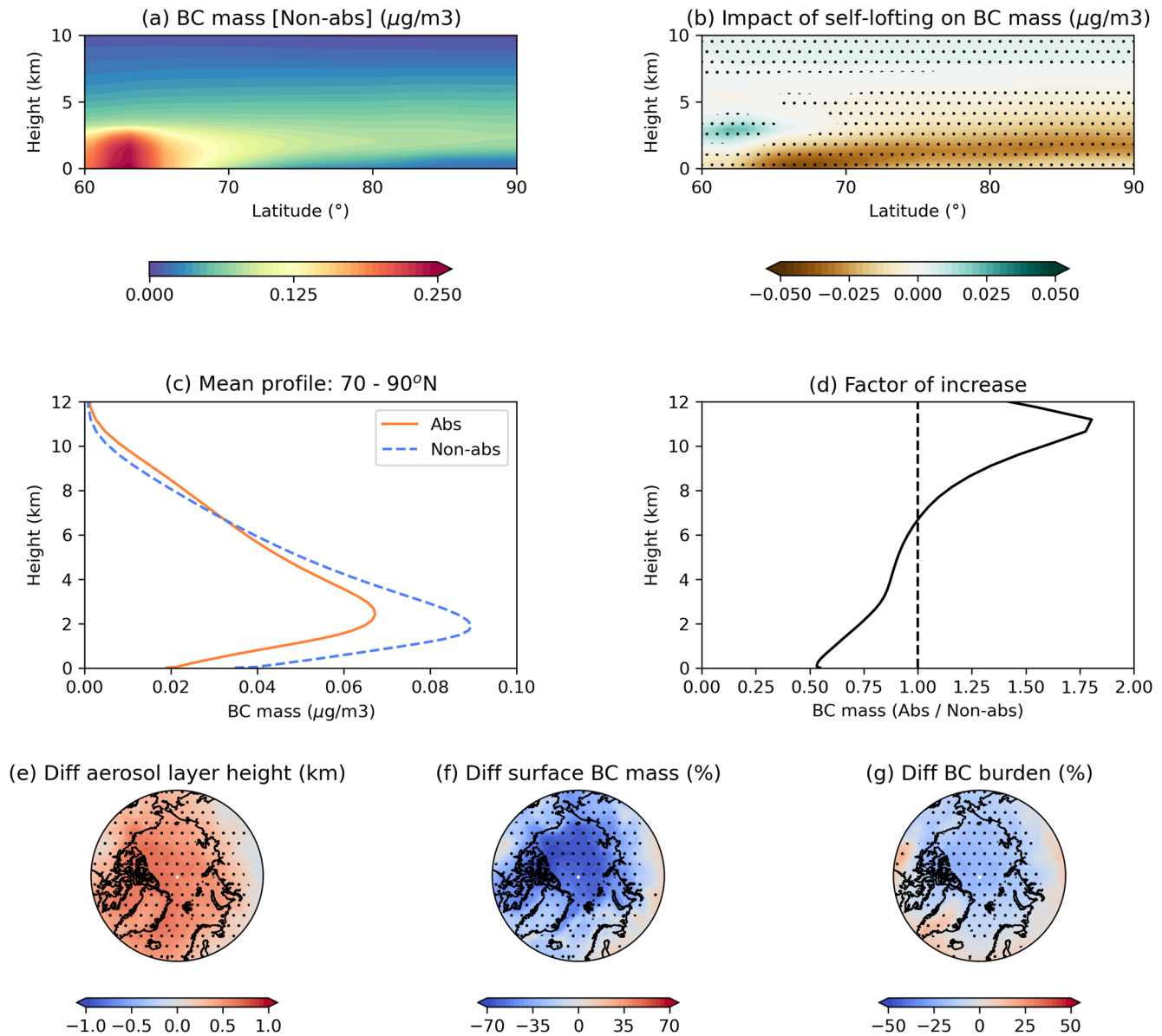


Figure 5. Impact of self-lofting on black carbon (BC) mass over the Arctic (60–90°N) during June–August. Plots include (a) zonal-mean concentration ($\mu\text{g}/\text{m}^3$) from the non-absorbing simulation, (b) the change due to self-lofting, (c) the mean vertical profiles of BC mass in the Abs and non-abs simulations for 70–90°N, (d) the ratio of the two profiles (Abs/Non-abs). Maps show the impact of self-lofting on (e) mean BC aerosol layer height (km), (f) the relative changes (%) in surface mass concentration and (g) BC column burden. Stipples indicate where the changes are statistically significant at the 95% confidence level.

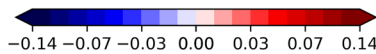
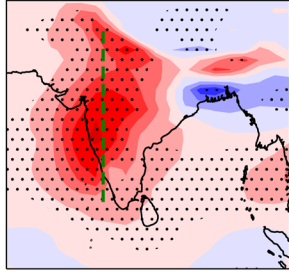
Reductions in BC surface concentrations imply a possible reduction in the deposition of BC on snow and the resulting snow-albedo effect. Decreasing haze in the lower troposphere could weaken aerosol-cloud interactions in low clouds. The effects of increasing BC in the upper troposphere and lower stratosphere are less clear but could include interactions with high altitude clouds and stratospheric heterogeneous chemistry.

4.3. Seasonal Response Over Southern Asia

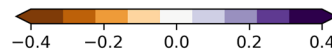
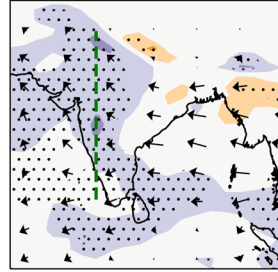
As indicated in Figure 1, high values of BC AAOD are found over Southern Asia and the associated atmospheric absorption clearly enhances vertical motion, even when evaluated on annual mean timescales. However, the impact on BC concentration at 3 km (Figure 1d) was weak or slightly negative in these regions raising the question as to what role absorption and self-lofting are having on aerosol transport in the region. BC absorption is understood to affect the Asian monsoon circulation in different ways in different seasons. The summer season is

DJF

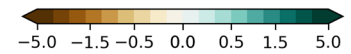
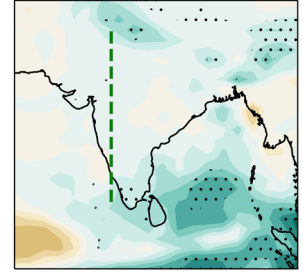
(a) Δ BC mass conc at 3km ($\mu\text{g}/\text{m}^3$)



(b) Δ W at 700mb (cm/s)

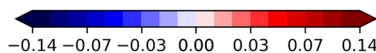
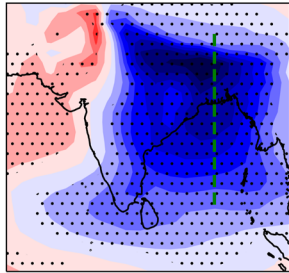


(c) Δ Precipitation (mm/day)

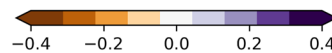
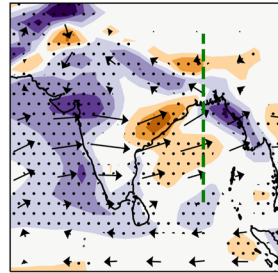


JJA

(d) Δ BC mass conc at 3km ($\mu\text{g}/\text{m}^3$)



(e) Δ W at 700mb (cm/s)



(f) Δ Precipitation (mm/day)

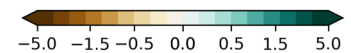
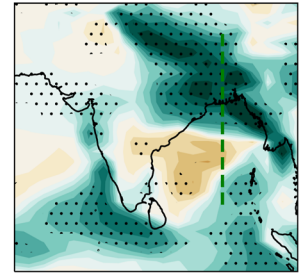


Figure 6. Impacts of black carbon (BC) absorption on self-lofting in the Southern Asia region. Plots include changes in BC mass at 3 km (a, d), vertical velocity and horizontal wind vectors at 700 mb (b, e), and precipitation (c, f), over southern Asia during DJF (top row) and JJA (bottom row). Vertical dashed lines indicate the cross-sections analyzed in Figure 7. Stipples indicate where the changes are statistically significant at the 95% confidence level.

characterized by inward flow to Southern Asia from the south-west and by deep convection that can be enhanced by aerosol absorption over the continent (e.g., Bollasina et al., 2008; Lau & Kim, 2006; Meehl et al., 2008). In winter the flow reverses and layers of absorbing aerosol build over the Indian sub-continent and are subsequently transported out in elevated layers over the Indian Ocean, as observed during the Indian Ocean Experiment (INDOEX) (e.g., Müller et al., 2003). One might expect the elevation of such layers to be influenced by self-lofting. The analysis in Figures 6 and 7 therefore look at the impact of BC self-lofting in both Boreal winter (DJF) and the summer (JJA) when the South Asian Monsoon is in opposite phases.

During DJF the inclusion of absorption leads to widespread increases of BC mass in the lower troposphere (Figure 6a), coherent with increases in vertical velocity at 700 mb (Figure 6b) indicating that self-lofting is aiding the transport of BC from the BL into the free troposphere. This is apparent over most of India and some parts of the Gangetic plain. The profiles and cross-sections in Figures 7a–7d indicate that aerosol is mainly confined to a layer 4 km deep over the Indian sub-continent with concentrations slightly higher at the northern end of the cross-section. The cross-section was positioned along 10–30°N, 76°E to intersect the region where the strongest relative increases in BC mass were found at 3 km (Figure 6a). The inclusion of absorption enhanced mass concentrations of BC throughout this layer, though the changes are not that large in relative terms (~5% below 2 km, rising to 25% at 4 km, Figure 7b). The BC absorption also induces an Easterly tendency in the 700 mb wind,

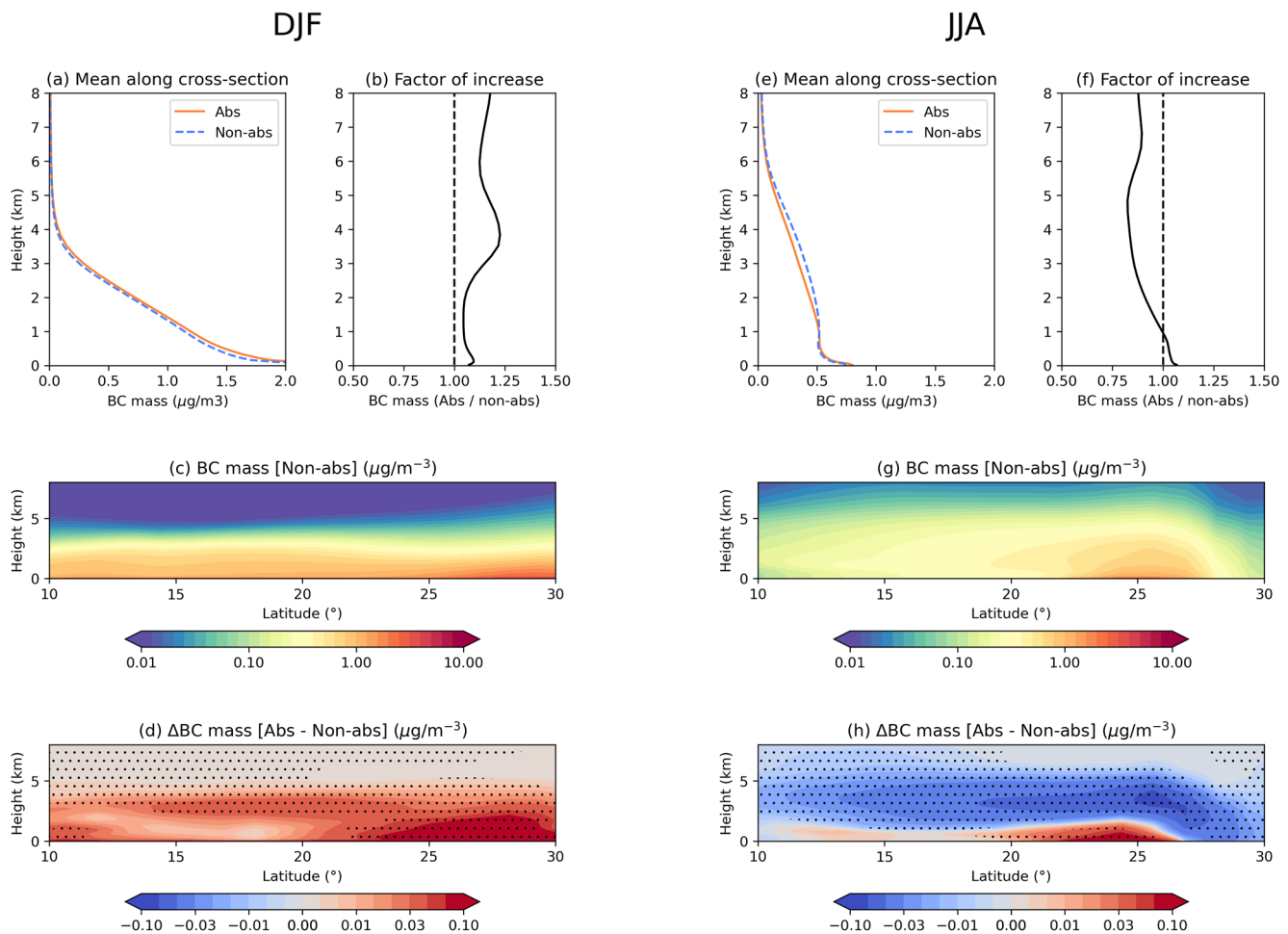


Figure 7. Changes to the vertical distribution of black carbon (BC) aerosol mass during December–February (DJF) and June–August (JJA) along a north-south cross-section along the western side of India (10° – 30° N, 75° E) for DJF and over the Bay of Bengal and Ganges delta (10° – 30° N, 90° E) for JJA (see dashed lines in Figure 6). Plots show seasonal mean BC mass concentration from the Abs and Non-abs simulations as either vertical profiles (a, e) or height-latitude distributions (c, g). Differences in BC mass between the Abs and Non-abs simulations are shown as both the factor of increase based on Abs/Non-abs (b, f) or the absolute change as a function of height and latitude (d, h). Stipples on plots d and h indicate where the changes are statistically significant at the 95% confidence level.

and this may explain why the enhancement in BC is stronger on the West side of the subcontinent. Precipitation is generally suppressed over Southern Asia during DJF and although there is enhanced ascent (or suppressed descent) this does not interfere significantly with precipitation patterns (Figure 6c) over the subcontinent.

A different pattern of feedbacks occurs during the summer season with the inclusion of absorption triggering reductions to BC mass at 3 km over most of Southern Asia and parts of the Indian Ocean (Figure 6d). As shown in Figures 7e–7h the BC mass concentrations are generally lower in the cross-section selected for this season (10 – 30° N, 90° E) but the mass is more evenly distributed in the vertical in this season. The position of this cross-section was selected to intersect the region where the strongest relative decreases in BC mass were found at 3 km (Figure 6d). Whilst the absorption does stimulate some areas of ascent in this season (Figure 6e) the pattern of circulation changes is more complex and the horizontal wind perturbations are more indicative of an enhancement to the Southwestern monsoon flow and cyclonic tendency over northeast India and the Bay of Bengal. Consistent with this there are large increases in precipitation with perturbations of up to 5 mm/day over parts of Southern Asia. The changes in BC concentration no longer correlate with changes in vertical motion (as they had in DJF) but rather the spatial pattern of reduced BC seems related to enhanced precipitation that is acting to wash the aerosol out. Indeed wet deposition averaged across the region in Figure 6 was 7% higher in the Abs simulation than Non-abs. The vertical profiles and the cross-section over the Indian Ocean (Figures 7e–7h) indicate that the absolute reduction of BC mass is greatest in the altitude range 1–6 km, where the losses due to wet deposition

were greatest in the model from the combination of nucleation scavenging and impaction scavenging and at the northern end of the cross-section where the precipitation increase was highest (Figure 6f). There were some increases in BC mass below 1 km but only slight, suggesting that the self-lofting was aiding the transport of BC up into the surface mixed layer, but above 1 km wet losses from in-cloud (nucleation) scavenging dominated. The feedback between enhanced ascent and wet deposition seems more important than the self-lofting effect during JJA and shows a more complex interplay of dynamical processes affecting the fate of aerosol in this region. In this case the lofting is somewhat self-limiting since it encourages the removal of the aerosol.

5. Conclusions

This study investigates the role that absorption plays in the vertical transport and global distribution of BC aerosol. This was examined using a pair of simulations with the UKESM1 Earth-system model where BC absorption either included or set to zero in the radiation calculation. Including absorption increased the ascent of BC into the free troposphere and lower stratosphere by enhancing large-scale vertical motion in regions with high BC loading and radiative absorption. This self-lofting process increased BC concentrations above 2 km (global mean) with the strongest increases of up to 50% in the upper troposphere and lower stratosphere (8–22 km). The increased elevation of BC aerosol also allowed it to travel further leading to increases in BC mass concentration in remote regions, including increases of 20%–40% at 3 km over many parts of the Pacific, South Atlantic and Indian Ocean and larger increases of up to 100% in the southeast Atlantic.

A significant upward shift in the vertical distribution of BC aerosol was also seen in certain regions, most notably the southeast Atlantic where the biomass burning aerosol plume over the ocean was up to 1 km higher in the simulation including BC absorption. This would likely have affected the overlap between the aerosol and marine boundary layer clouds and the simulation of radiative forcing and aerosol-cloud microphysical interactions in the region, although such follow-on impacts were not investigated here. Other regions heavily affected by biomass burning (southern Asia, Indonesia, Amazonia, and northern high latitudes) generally showed enhanced BC concentrations within and downwind of the aerosol sources.

The Arctic region was similarly affected with the absorption leading to a further 0.5–1 km in the elevation of absorbing haze layers in the mid-troposphere. The self-lofting also reduced surface concentrations of BC by around 50%. This could imply less BC deposition on the snow/ice surfaces affecting any “BC on snow” forcing, although BC-snow albedo effects were not represented in this model configuration. BC concentrations in the lower stratosphere also increased, on average by a factor of 1.7 in the summer season as a result of the dynamical responses to BC absorption.

Different feedbacks were seen over the Indian subcontinent during the summer monsoon. Whilst the heavy loading of BC over Southern Asia generally enhanced vertical motion in the region, during the wet season (June–August) this increased precipitation and reduced BC loading via wet deposition. During the winter dry season the feedback on precipitation was much weaker or absent and the response was similar to that seen elsewhere with absorption generally enhancing BC concentrations in the free troposphere.

In summary, in this model BC absorption has a wide range of effects on the transport and distribution of aerosols at global and regional scales. Accurately representing the level of BC absorption in atmospheric models is therefore important not just to simulate the radiative interaction itself but also to simulate transport processes and the vertical distribution. We recommend further investigation to assess how self-lofting alters aerosol forcings in sensitive regions such as the southeast Atlantic.

Data Availability Statement

All simulation data used in this study were created by the UK Earth System Model (UKESM1), a configuration of the Met Office Unified Model (UM). The UK Earth System model is documented in Sellar et al. (2019). The model outputs and software programs used in this study are accessible via the zenodo repository <https://doi.org/10.5281/zenodo.7152687>. Due to intellectual property right restrictions, we cannot provide the source code or documentation papers for the UM. The Met Office Unified Model is available for use under licence. A number of research organizations and national meteorological services use the UM in collaboration with the Met Office to undertake basic atmospheric process research, produce forecasts, develop the UM code, and build and

evaluate Earth system models. For further information on how to apply for a licence, see <http://www.metoffice.gov.uk/research/modelling-systems/unified-model>.

Acknowledgments

Ben Johnson and Jim Haywood were funded under the joint UK BEIS/DEFRA—Met Office Hadley Centre Climate Programme (GA01101). JH would like to acknowledge support from the NERC funded SASSO standard Grant (NE/S00212X/1).

References

- Ackerman, A. S., Toon, O. B., Stevens, D. E., Heymsfield, A. J., Ramanathan, V., & Welton, E. J. (2000). Reduction of tropical cloudiness by soot. *Science*, *288*(5468), 1042–1047. <https://doi.org/10.1126/science.288.5468.1042>
- Ajoku, O., Norris, J. R., & Miller, A. J. (2019). Observed monsoon precipitation suppression caused by anomalous interhemispheric aerosol transport. *Climate Dynamics*, *54*(1–2), 1077–1091. <https://doi.org/10.1007/s00382-019-05046-y>
- Allen, R. J., Sherwood, S. C., Norris, J. R., & Zender, C. S. (2012). Recent Northern Hemisphere tropical expansion primarily driven by black carbon and tropospheric ozone. *Nature*, *485*(7398), 350–354. <https://doi.org/10.1038/nature11097>
- Ansmann, A., Ohneiser, K., Chudnovsky, A., Baars, H., & Engelmann, R. (2021). CALIPSO aerosol-typing scheme misclassified stratospheric fire smoke: Case study from the 2019 Siberian wildfire season. *Frontiers in Environmental Science*, *9*, 769852. <https://doi.org/10.3389/fevs.2021.769852>
- Boers, R., de Laat, A. T., Stein Zweers, D. C., & Dirksen, R. J. (2010). Lifting potential of solar-heated aerosol layers. *Geophysical Research Letters*, *37*, L24802. <https://doi.org/10.1029/2010GL045171>
- Bollasina, M., Nigam, S., & Lau, K.-M. (2008). Absorbing aerosols and summer monsoon evolution over South Asia: An observational portrayal. *Journal of Climate*, *21*(13), 3221–3239. <https://doi.org/10.1175/2007JCLI12094.1>
- Bond, T. C., & Bergstrom, R. W. (2006). Light absorption by carbonaceous particles: An investigative review. *Aerosol Science and Technology*, *40*(1), 27–67. <https://doi.org/10.1080/02786820500421521>
- Bond, T. C., Doherty, S. J., Fahey, D. W., Forster, P. M., Berntsen, T., DeAngelo, B. J., et al. (2013). Bounding the role of black carbon in the climate system: A scientific assessment. *Journal of Geophysical Research: Atmospheres*, *118*(11), 5380–5552. <https://doi.org/10.1002/jgrd.50171>
- Boone, C. D., Bernath, P. F., Labelle, K., & Crouse, J. (2022). Stratospheric aerosol composition observed by the atmospheric chemistry experiment following the 2019 Raikoke eruption. *Journal of Geophysical Research: Atmospheres*, *127*(18), e2022JD036600. <https://doi.org/10.1029/2022jd036600>
- Collins, W. J., Lamarque, J.-F., Schulz, M., Boucher, O., Eyring, V., Hegglin, M. I., et al. (2017). AerChemMIP: Quantifying the effects of chemistry and aerosols in CMIP6. *Geoscientific Model Development*, *10*(2), 585–607. <https://doi.org/10.5194/gmd-10-585-2017>
- Damany-Pearce, L., Johnson, B., Wells, A., Osborne, M., Allan, J., Belcher, C., et al. (2022). Australian wildfires cause the largest stratospheric warming since Pinatubo and extends the lifetime of the Antarctic ozone hole. *Scientific Reports*, *12*(1), 12665. <https://doi.org/10.1038/s41598-022-15794-3>
- de Graaf, M., Schulte, R., Peers, F., Waquet, F., Tilstra, L. G., & Stammes, P. (2020). Comparison of South-East Atlantic aerosol direct radiative effect over clouds from SCIAMACHY, POLDER and OMI–MODIS. *Atmospheric Chemistry and Physics*, *20*(11), 6707–6723. <https://doi.org/10.5194/acp-20-6707-2020>
- Edwards, J. M., & Slingo, A. (1996). Studies with a flexible new radiation code. I: Choosing a configuration for a large-scale model. *Quarterly Journal of Royal Meteorological Society*, *122*(531), 689–719. <https://doi.org/10.1002/qj.49712253107>
- Frierson, D. M., Hwang, Y.-T., Fučkar, N. S., Seager, R., Kang, S. M., Donohoe, A., et al. (2013). Contribution of ocean overturning circulation to tropical rainfall peak in the Northern Hemisphere. *Nature Geoscience*, *6*(11), 940–944. <https://doi.org/10.1038/ngeo1987>
- Ghan, S. J., Liu, X., Easter, R. C., Zaveri, R., Rasch, P. J., Yoon, J., & Eaton, B. (2012). Toward a minimal representation of aerosols in climate models: Comparative decomposition of aerosol direct, semidirect, and indirect radiative forcing. *Journal of Climate*, *25*(19), 6461–6476. <https://doi.org/10.1175/JCLI-D-11-00650.1>
- Gupta, S., McFarquhar, G. M., O'Brien, J. R., Delene, D. J., Poellot, M. R., Dobracki, A., et al. (2021). Impact of the variability in vertical separation between biomass burning aerosols and marine stratocumulus on cloud microphysical properties over the Southeast Atlantic. *Atmospheric Chemistry and Physics*, *21*(6), 4615–4635. <https://doi.org/10.5194/acp-21-4615-2021>
- Hawcroft, M., Haywood, J. M., Collins, M., Jones, A., Jones, A. C., & Stephens, G. (2017). Southern Ocean albedo, inter-hemispheric energy transports and the double ITCZ: Global impacts of biases in a coupled model. *Climate Dynamics*, *48*(7–8), 2279–2295. <https://doi.org/10.1007/s00382-016-3205-5>
- Haywood, J. M., Abel, S. J., Barrett, P. A., Bellouin, N., Blyth, A., Bower, K. N., et al. (2021). The CLoud–aerosol–radiation interaction and forcing: Year 2017 (CLARIFY-2017) measurement campaign. *Atmospheric Chemistry and Physics*, *21*(2), 1049–1084. <https://doi.org/10.5194/acp-21-1049-2021>
- Haywood, J. M., Jones, A., Bellouin, N., & Stephenson, D. B. (2013). Asymmetric forcing from stratospheric aerosols impacts Sahelian drought. *Nature Climate Change*, *3*(7), 660–665. <https://doi.org/10.1038/NCLIMATE1857>
- Haywood, J. M., Jones, A., Dunstone, N., Milton, S., Vellinga, M., Bodas-Salcedo, A., et al. (2016). The impact of equilibrating hemispheric albedos on tropical performance in the HadGEM2-ES coupled climate model. *Geophysical Research Letters*, *43*(1), 395–403. <https://doi.org/10.1002/2015GL066903>
- Haywood, J. M., Jones, A., Johnson, B. T., & McFarlane Smith, W. (2022). Assessing the consequences of including aerosol absorption in potential stratospheric aerosol injection climate intervention strategies. *Atmospheric Chemistry and Physics*, *22*(9), 6135–6150. <https://doi.org/10.5194/acp-22-6135-2022>
- Herbert, R. J., Bellouin, N., Highwood, E. J., & Hill, A. A. (2020). Diurnal cycle of the semi-direct effect from a persistent absorbing aerosol layer over marine stratocumulus in large-eddy simulations. *Atmospheric Chemistry and Physics*, *20*(3), 1317–1340. <https://doi.org/10.5194/acp-20-1317-2020>
- Herring, J. A., & Hobbs, P. V. (1994). Radiatively driven dynamics of the plume from 1991 Kuwait oil fires. *Journal of Geophysical Research*, *99*(D9), 18809–18826. <https://doi.org/10.1029/94JD01753>
- Hoesly, R. M., Smith, S. J., Feng, L., Klimont, Z., Janssens-Maenhout, G., Pitkanen, T., et al. (2018). Historical (1750–2014) anthropogenic emissions of reactive gases and aerosols from the Community Emissions Data System (CEDS). *Geoscientific Model Development*, *11*(1), 369–408. <https://doi.org/10.5194/gmd-11-369-2018>
- Hwang, Y. T., & Frierson, D. M. (2013). Link between the double-intertropical convergence zone problem and cloud biases over the Southern Ocean. *Proceedings of the National Academy of Sciences of the United States of America*, *110*(13), 4935–4940. <https://doi.org/10.1073/pnas.1213302110>
- Johnson, B. T. (2022). Data and software in support of article submitted to Journal Geophys. Res. Atmos., titled "Assessing the impact of self-lofting on increasing the altitude of black carbon in a global climate model". [Dataset]. Zenodo. <https://doi.org/10.5281/zenodo.7152687>

- Johnson, B. T., Haywood, J. M., & Hawcroft, M. K. (2019). Are changes in atmospheric circulation important for black carbon aerosol impacts on clouds, precipitation, and radiation? *Journal of Geophysical Research: Atmospheres*, *124*(14), 7930–7950. <https://doi.org/10.1029/2019JD030568>
- Johnson, B. T., Shine, K. P., & Forster, P. M. (2004). The semi-direct aerosol effect: Impact of absorbing aerosols on marine stratocumulus. *Quarterly Journal of Royal Meteorological Society*, *130*(599), 1407–1422. <https://doi.org/10.1256/qj.03.61>
- Kablick, G. P., Allen, D. R., Fromm, M. D., & Nedoluha, G. E. (2020). Australian pyroCb smoke generates synoptic-scale stratospheric anticyclones. *Geophysical Research Letters*, *47*(13), e2020GL088101. <https://doi.org/10.1029/2020gl088101>
- Kang, S., Zhang, Y., Qian, Y., & Wang, H. (2020). A review of black carbon in snow and ice and its impact on the cryosphere. *Earth-Science Reviews*, *210*, 103346. <https://doi.org/10.1016/j.earscirev.2020.103346>
- Keil, A., & Haywood, J. M. (2003). Solar radiative forcing by biomass burning aerosol particles during SAFARI 2000: A case study based on measured aerosol and cloud properties. *Journal of Geophysical Research*, *108*(D13), 8467. <https://doi.org/10.1029/2002JD002315>
- Khaykin, S., Legras, B., Bucci, S., Sellitto, P., Isaksen, I., Tencé, F., et al. (2020). The 2019/20 Australian wildfires generated a persistent smoke-charged vortex rising up to 35 km altitude. *Nature Communications Earth and Environment*, *1*, 22. <https://doi.org/10.1038/s43247-020-00022-5>
- Koch, D., & Del Genio, A. D. (2010). Black carbon semi-direct effects on cloud cover: Review and synthesis. *Atmospheric Chemistry and Physics*, *10*(16), 7685–7696. <https://doi.org/10.5194/acp-10-7685-2010>
- Kovilakam, M., & Mahajan, S. (2015). Black carbon aerosol-induced Northern Hemisphere tropical expansion. *Geophysical Research Letters*, *42*(12), 4964–4972. <https://doi.org/10.1002/2015GL064559>
- Kuhbrodt, T., Jones, C. G., Sellar, A., Storkey, D., Blockley, E., Stringer, M., et al. (2018). The low-resolution version of HadGEM3 GC3.1: Development and evaluation for global climate. *Journal of Advances in Modeling Earth Systems*, *10*(11), 2865–2888. <https://doi.org/10.1029/2018MS001370>
- Laat, A. T. J., Stein Zweers, D. C., Boers, R., & Tuinder, O. N. E. (2012). A solar escalator: Observational evidence of the self-lifting of smoke and aerosols by absorption of solar radiation in the February 2009 Australian Black Saturday plume. *Journal of Geophysical Research*, *117*, D04204. <https://doi.org/10.1029/2011JD017016>
- Lau, K.-M., & Kim, K.-M. (2006). Observational relationships between aerosol and Asian monsoon rainfall, and circulation. *Geophysical Research Letters*, *33*(21), L21810. <https://doi.org/10.1029/2006GL027546>
- Law, K. S., & Stohl, A. (2007). Arctic air pollution: Origins and impacts. *Science*, *315*(5818), 1537–1540. <https://doi.org/10.1126/science.1137695>
- Lohmann, U. (2017). Anthropogenic aerosol influences on mixed-phase clouds. *Current Climate Change Reports*, *3*(1), 32–44. <https://doi.org/10.1007/s40641-017-0059-9>
- Mallet, M., Solmon, F., Nabat, P., Elguindi, N., Waquet, F., Bouniol, D., et al. (2020). Direct and semi-direct radiative forcing of biomass-burning aerosols over the southeast Atlantic (SEA) and its sensitivity to absorbing properties: A regional climate modeling study. *Atmospheric Chemistry and Physics*, *20*(21), 13191–13216. <https://doi.org/10.5194/acp-20-13191-2020>
- Mann, G. W., Carslaw, K. S., Spracklen, D. V., Ridley, D. A., Manktelow, P. T., Chipperfield, M. P., et al. (2010). Description and evaluation of GLOMAP-mode: A modal global aerosol microphysics model for the UKCA composition-climate model. *Geoscientific Model Development*, *3*(2), 519–551. <https://doi.org/10.5194/gmd-3-519-2010>
- Manners, J., Edwards, J. M., Hill, P., & Thelen, J.-C. (2022). SOCRATES technical guide (Suite Of Community RAdiative Transfer codes based on Edwards and Slingo). Met Office, UK. Retrieved from <https://code.metoffice.gov.uk/trac/socrates>
- Meehl, G. A., Arblaster, J. M., & Collins, W. D. (2008). Effects of black carbon aerosols on the Indian Monsoon. *Journal of Climate*, *21*(12), 2869–2882. <https://doi.org/10.1175/2007JCLI1777.1>
- Ming, Y., Ramaswamy, V., & Persad, G. (2010). Two opposing effects of absorbing aerosols on global-mean precipitation. *Geophysical Research Letters*, *37*(13), L13701. <https://doi.org/10.1029/2010GL042895>
- Moorthy, K. K., Satheesh, S. K., & Kotamarthi, V. R. (2016). Evolution of aerosol research in India and the RAWEX–GVAX: An overview. *Current Science*, *111*(1), 53–75. <https://doi.org/10.18520/cs/v111/i1/53-75>
- Mulcahy, J. P., Johnson, C., Jones, C. G., Povey, A. C., Scott, C. E., Sellar, A., et al. (2020). Description and evaluation of aerosol in UKESM1 and HadGEM3-GC3.1 CMIP6 historical simulations. *Geoscientific Model Development*, *13*(12), 6383–6423. <https://doi.org/10.5194/gmd-13-6383-2020>
- Mulcahy, J. P., Jones, C., Sellar, A., Johnson, B., Boutle, I. A., Jones, A., et al. (2018). Improved aerosol processes and effective radiative forcing in HadGEM3 and UKESM1. *Journal of Advances in Modeling Earth Systems*, *10*(11), 2786–2805. <https://doi.org/10.1029/2018MS001464>
- Müller, D., Franke, K., Ansmann, A., Althausen, D., & Wagner, F. (2003). Indo-Asian pollution during INDOEX: Microphysical particle properties and single-scattering albedo inferred from multiwavelength lidar observations. *Journal of Geophysical Research*, *108*(D19), 4600. <https://doi.org/10.1029/2003JD003538>
- Muser, L. O., Hoshyaripour, G. A., Bruckert, J., Horváth, Á., Malinina, E., Wallis, S., et al. (2020). Particle aging and aerosol–radiation interaction affect volcanic plume dispersion: Evidence from the Raikoke 2019 eruption. *Atmospheric Chemistry and Physics*, *20*(23), 15015–15036. <https://doi.org/10.5194/acp-20-15015-2020>
- Myhre, G., Kramer, R. J., Smith, C. J., Hodnebrog, Ø., Forster, P., Soden, B. J., et al. (2018). Quantifying the importance of rapid adjustments for global precipitation changes. *Geophysical Research Letters*, *45*(20), 11399–11405. <https://doi.org/10.1029/2018GL079474>
- Myhre, G., Samset, B. H., Schulz, M., Balkanski, Y., Bauer, S., Bernsten, T. K., et al. (2013). Radiative forcing of the direct aerosol effect from AeroCom Phase II simulations. *Atmospheric Chemistry and Physics*, *13*(4), 1853–1877. <https://doi.org/10.5194/acp-13-1853-2013>
- O'Connor, F. M., Abraham, N. L., Dalvi, M., Folberth, G. A., Griffiths, P. T., Hardacre, C., et al. (2021). Assessment of pre-industrial to present-day anthropogenic climate forcing in UKESM1. *Atmospheric Chemistry and Physics*, *21*(2), 1211–1243. <https://doi.org/10.5194/acp-21-1211-2021>
- Ohneiser, K., Ansmann, A., Chudnovsky, A., Engelmann, R., Ritter, C., Veselovskii, I., et al. (2021). The unexpected smoke layer in the High Arctic winter stratosphere during MOSAiC 2019–2020. *Atmospheric Chemistry and Physics*, *21*(20), 15783–15808. <https://doi.org/10.5194/acp-21-15783-2021>
- Ohneiser, K., Ansmann, A., Witthuhn, J., Deneke, H., Chudnovsky, A., Walter, G., & Senf, F. (2023). Self-lofting of wildfire smoke in the troposphere and stratosphere: Simulations and space lidar observations. *Atmospheric Chemistry and Physics*, *23*, 2901–2925. <https://doi.org/10.5194/acp-23-2901-2023>
- Pausata, F. S. R., Lindvall, J., Ekman, A. M. L., & Svensson, G. (2016). Climate effects of a hypothetical regional nuclear war: Sensitivity to emission duration and particle composition. *Earth's Future*, *4*(11), 498–511. <https://doi.org/10.1002/2016EF000415>
- Peterson, D. A., Campbell, J. R., Hyer, E. J., Fromm, M. D., Kablick, G. P., Cossuth, J. H., & DeLand, M. T. (2018). Wildfire-driven thunderstorms cause a volcano-like stratospheric injection of smoke. *npj Climate and Atmospheric Science*, *1*, 30. <https://doi.org/10.1038/s41612-018-0039-3>

- Quinn, P. K., Shaw, G., Andrews, E., Dutton, E. G., Ruoho-Airola, T., & Gong, S. L. (2007). Arctic haze: Current trends and knowledge gaps. *Tellus B*, 59(1), 99–114. <https://doi.org/10.1111/j.1600-0889.2006.00236.x>
- Radke, L. F., Lyons, J. H., Hobbs, P. V., & Weiss, R. E. (1990). Smokes from the burning of aviation fuel and their self-lifting by solar heating. *Journal of Geophysical Research*, 95(D9), 14071–14076. <https://doi.org/10.1029/JD095iD09p14071>
- Ramanathan, V., & Carmichael, G. (2008). Global and regional climate changes due to black carbon. *Nature Geoscience*, 1(4), 221–227. <https://doi.org/10.1038/ngeo156>
- Randles, C., & Ramaswamy, V. (2010). Direct and semi-direct impacts of absorbing biomass burning aerosol on the climate of southern Africa: A geophysical fluid dynamics laboratory GCM sensitivity study. *Atmospheric Chemistry and Physics*, 10(20), 9819–9831. <https://doi.org/10.5194/acp-10-9819-2010>
- Redemann, J., Wood, R., Zuidema, P., Doherty, S. J., Luna, B., LeBlanc, S. E., et al. (2021). An overview of the ORACLES (ObseRvations of Aerosols above CLouds and their intERactionS) project: Aerosol–cloud–radiation interactions in the southeast Atlantic basin. *Atmospheric Chemistry and Physics*, 21(3), 1507–1563. <https://doi.org/10.5194/acp-21-1507-2021>
- Sakaeda, N., Wood, R., & Rasch, P. J. (2011). Direct and semidirect aerosol effects of southern African biomass burning aerosol. *Journal of Geophysical Research*, 116(D12), D12205. <https://doi.org/10.1029/2010JD015540>
- Samsat, B. H., & Myhre, G. (2015). Climate response to externally mixed black carbon as a function of altitude. *Journal of Geophysical Research: Atmospheres*, 120(7), 2913–2927. <https://doi.org/10.1002/2014JD022849>
- Samsat, B. H., Myhre, G., Forster, P. M., Hodnebrog, Ø., Andrews, T., Faluvegi, G., et al. (2016). Fast and slow precipitation responses to individual climate forcings: A PDRMIP multimodel study. *Geophysical Research Letters*, 43(6), 2782–2791. <https://doi.org/10.1002/2016GL068064>
- Sand, M., Iversen, T., Bohlinger, P., Kirkevåg, A., Seierstad, I., Seland, Ø., & Sorteberg, A. (2015). A Standardized global climate model study showing unique properties for the climate response to black carbon aerosols. *Journal of Climate*, 28(6), 2512–2526. <https://doi.org/10.1175/JCLI-D-14-00050.1>
- Sellar, A. A., Jones, C. G., Mulcahy, J. P., Tang, Y., Yool, A., Wiltshire, A., et al. (2019). UKESM1: Description and evaluation of the U.K. Earth System Model. *Journal of Advances in Modeling Earth Systems*, 11(12), 4513–4558. <https://doi.org/10.1029/2019MS001739>
- Sellar, A. A., Walton, J., Jones, C. G., Wood, R., Abraham, N. L., Andrejczuk, M., et al. (2020). Implementation of U.K. Earth system models for CMIP6. *Journal of Advances in Modeling Earth Systems*, 12(4), e2019MS001946. <https://doi.org/10.1029/2019MS001946>
- Shaw, G. E. (1995). The Arctic haze phenomenon. *Bulletin of the American Meteorological Society*, 76(12), 2403–2414. [https://doi.org/10.1175/1520-0477\(1995\)076<2403:TAHP>2.0.CO;2](https://doi.org/10.1175/1520-0477(1995)076<2403:TAHP>2.0.CO;2)
- Shen, Z., & Ming, Y. (2018). The influence of aerosol absorption on the extratropical circulation. *Journal of Climate*, 31(15), 5961–5975. <https://doi.org/10.1175/JCLI-D-17-0839.1>
- Smith, C. J., Kramer, R. J., Myhre, G., Forster, P. M., Soden, B. J., Andrews, T., et al. (2018). Understanding rapid adjustments to diverse forcing agents. *Geophysical Research Letters*, 45(21), 12023–12031. <https://doi.org/10.1029/2018GL079826>
- Solmon, F., Elguindi, N., Mallet, M., Flamant, C., & Formenti, P. (2021). Modulation of West African Monsoon precipitation by central and southern African biomass aerosol emissions. *npj Climate and Atmospheric Science*, 4(1), 54. <https://doi.org/10.1038/s41612-021-00210-w>
- Stjern, C. W., Samsat, B. H., Myhre, G., Forster, P. M., Hodnebrog, Ø., Andrews, T., et al. (2017). Rapid adjustments cause weak surface temperature response to increased black carbon concentrations. *Journal of Geophysical Research: Atmospheres*, 122(21), 11462–11481. <https://doi.org/10.1002/2017JD027326>
- Stohl, A., Klimont, Z., Eckhardt, S., Kupiainen, K., Shevchenko, V. P., Kopeikin, V. M., & Novigatsky, A. N. (2013). Black carbon in the Arctic: The underestimated role of gas flaring and residential combustion emissions. *Atmospheric Chemistry and Physics*, 13(17), 8833–8855. <https://doi.org/10.5194/acp-13-8833-2013>
- Torres, O., Bhartia, P. K., Taha, G., Jethva, H., Das, S., Colarco, P., et al. (2020). Stratospheric injection of massive smoke plume from Canadian boreal fires in 2017 as seen by DSCOVR-EPIC, CALIOP, and OMPs-LP observations. *Journal of Geophysical Research: Atmospheres*, 125(10), e2020JD032579. <https://doi.org/10.1029/2020jd032579>
- Voigt, A., Stevens, B., Bader, J., & Mauritsen, T. (2013). The observed hemispheric symmetry in reflected shortwave irradiance. *Journal of Climate*, 26(2), 468–477. <https://doi.org/10.1175/jcli-d-12-00132.1>
- Voigt, A., Stevens, B., Bader, J., & Mauritsen, T. (2014). Compensation of hemispheric albedo asymmetries by shifts of the ITCZ and tropical clouds. *Journal of Climate*, 27(3), 1029–1045. <https://doi.org/10.1175/jcli-d-13-00205.1>
- Wang, C. (2013). Impact of anthropogenic absorbing aerosols on clouds and precipitation (2013), A review of recent progresses. *Atmospheric Research*, 122, 237–249. <https://doi.org/10.1016/j.atmosres.2012.11.005>
- West, R. E. L., Stier, P., Jones, A., Johnson, C. E., Mann, G. W., Bellouin, N., & Kipling, Z. (2014). The importance of vertical velocity variability for estimates of the indirect aerosol effects. *Atmospheric Chemistry and Physics*, 14(12), 6369–6393. <https://doi.org/10.5194/acp-14-6369-2014>
- Williams, K. D., Copsey, D., Blockley, E. W., Bodas-Salcedo, A., Calvert, D., Comer, R., et al. (2018). The Met Office global coupled model 3.0 and 3.1 (GC3.0 and GC3.1) configurations. *Journal of Advances in Modeling Earth Systems*, 10(2), 357–380. <https://doi.org/10.1002/2017MS001115>
- WMO. (1992). *International meteorological vocabulary* (2nd ed., pp. 636–637). Secretariat of the World Meteorological Organization.
- Woodward, S., Sellar, A. A., Tang, Y., Stringer, M., Yool, A., Robertson, E., & Wiltshire, A. (2022). The simulation of mineral dust in the United Kingdom Earth System Model UKESM1. *Atmospheric Chemistry and Physics*, 22(22), 14503–14528. <https://doi.org/10.5194/acp-22-14503-2022>
- Xian, P., Zhang, J., O'Neill, N. T., Reid, J. S., Toth, T. D., Sorenson, B., et al. (2022). Arctic spring and summertime aerosol optical depth baseline from long-term observations and model reanalyses – Part 2: Statistics of extreme AOD events, and implications for the impact of regional biomass burning processes. *Atmospheric Chemistry and Physics*, 22(15), 9949–9967. <https://doi.org/10.5194/acp-22-9949-2022>
- Yu, P., Davis, S. M., Toon, O. B., Portmann, R. W., Bardeen, C. G., Barnes, J. E., et al. (2021). Persistent stratospheric warming due to 2019–2020 Australian wildfire smoke. *Geophysical Research Letters*, 48(7), e2021GL092609. <https://doi.org/10.1029/2021GL092609>
- Yu, P., Toon, O. B., Bardeen, C. G., Zhu, Y., Rosenlof, K. H., Portmann, R. W., et al. (2019). Black carbon lifts wildfire smoke high into the stratosphere to form a persistent plume. *Science*, 365(6453), 587–590. <https://doi.org/10.1126/science.aax1748>
- Zarzycki, C. M., & Bond, T. C. (2010). How much can the vertical distribution of black carbon affect its global direct radiative forcing? *Geophysical Research Letters*, 37(20), L20807. <https://doi.org/10.1029/2010GL044555>
- Zhang, H., & Wang, Z. (2011). Advances in the study of black carbon effects on climate. *Advances in Climate Change Research*, 2(1), 23–30. <https://doi.org/10.3724/SP.J.1248.2011.00023>
- Zheng, C., Wu, Y., Ting, M., Orbe, C., Wang, X., & Tilmes, S. (2021). Summertime transport pathways from different Northern Hemisphere regions into the Arctic. *Journal of Geophysical Research: Atmospheres*, 126(4), e2020JD033811. <https://doi.org/10.1029/2020JD033811>